Hindawi Publishing Corporation
Mathematical Problems in Engineering
Volume 2015, Article ID 905731, 15 pages
http://dx.doi.org/10.1155/2015/905731

Research Article

Method for Modeling Electrorheological Dampers Using Its Dynamic Characteristics

Carlos A. Vivas-Lopez, Diana Hernández-Alcantara, Ruben Morales-Menendez, Ricardo A. Ramírez-Mendoza, and Horacio Ahuett-Garza

ITESM Campus Monterrey, Avenue Eugenio Garza Sada 2501, Col. Tecnológico, 64849 Monterrey, NL, Mexico

Correspondence should be addressed to Carlos A. Vivas-Lopez; a00794204@itesm.mx

Received 6 June 2014; Accepted 30 August 2014

Academic Editor: Xingsheng Gu

A method for modeling an *Electrorheological* (ER) damper is proposed. The modeling method comprehends two simple steps: characterization and model customization. These steps are based on the experimental data of the damper behavior. Experiments were designed to explore the nonlinear behavior of the damper at different frequencies and actuation signals (i.e., automotive domain). The resulting model has low computational complexity. The method was experimentally validated with a commercial damper. The *error-to-signal Ratio* (ESR) performance index was used to evaluate the model accuracy. The results were quantitatively compared with two well-known ER damper models: the *Choi* parametric model and the *Eyring-plastic* model. The new proposed model has a 44% better ESR index than the *Choi* parametric model and 28% for the *Eyring-plastic* model. A qualitative comparison based on density plots highlights the advantages of this proposal.

1. Introduction

In an automotive suspension system the shock absorber has the purpose of dissipating the energy of the motion of the vehicle caused by the road disturbances. This energy dissipation allows the suspension to achieve two important objectives: decrease the vertical acceleration and maintain the tires in contact with the ground. Passive suspension systems are tailored to achieve a tradeoff of these objectives [1]. Semiactive (SA) suspension systems use a particular type of shock absorber which is capable of online modifying the amount of energy that can dissipate. This change on the damper needs to be controlled, to achieve the desired objectives.

The electrorheological (ER) damper is a hydraulic device, which is filled with a mixture of low viscosity oil and particles that are sensitive to an electric field. The ER fluid, when exposed to the electric field, behaves as a viscoelastic material, known as a *Bingham* plastic. This means that ideally it behaves as a solid at low stress efforts, but it flows as a viscous fluid when this force reaches its yield stress. Furthermore, the yield stress is field dependent; it increases as the electric field does.

An accurate mathematical model to predict the nonlinear dynamic behavior of the ER damper is needed in order to get a better control of the SA suspension system. There are several contributions in this topic [2, 3]. However, most of them are highly dependent on internal physical properties of the damper (usually confidential information), demand too much computational effort, or fail to capture the nonlinear behavior of the ER damper.

A new method to model an ER damper is proposed. The method comprehends two main steps: (1) a characterization procedure where the dynamical response of the damper is analyzed and (2) a model customization where a general model is tailored. This method requires experimental data of the ER damper. The resulting model is light enough to be implemented in an embedded system. The method is validated with intensive experimental data and compared to others published.

This paper is organized as follows: in Section 2 a bibliographic review of ER damper modeling is presented. In Section 3 the experimental system and the *Design of Experiments* (DoE) are shown. Section 4 describes the proposed method. Section 5 presents the modeling procedure.

Section 6 shows the results and evaluates the performance of the customized model. Finally, Section 7 concludes the paper.

2. ER Damper Models: State of the Art

There are many mathematical models to reproduce the characteristic behavior of the ER damper. The major efforts have been aimed at parametric models. [4] proposes a model based on the viscoelastic characteristics of the ER damper; this model contemplates a linear passive damping force that depends on the piston velocity and a lineal SA effect that only depends on the electric field applied to the ER fluid, this is a simple model that does not contemplate hysteresis and the damping force is completely linear.

A model based on the pressure drop in the ER channel is presented by [5]; this pressure drop considers an effect that depends on the damper velocity and others that just depend on the electric field; the coefficients for this model are based on physical dimensions of the damper and physical properties of the ER fluid. [6] proposes a model using a bond graph to model de governing equation of motion of the damper, but the physical dimensions and properties of the damper and ER fluid are needed. Later [7] shows two different types of ER damper configurations. The first one is the most common, the cylindrical type, in which the ER fluid flows through an annular channel where the electric field is applied. The second one is the orifice type; this type has a mechanism located inside the piston of the damper, which regulates the flow of the ER fluid through its chambers; two models were proposed, one for each type of damper, but the ones of physical parameters are needed.

Following the same line in terms of parametric models, [8] describes a hydromechanical based model. This model divides the damper in different zones where the pressure drop is calculated and the damper force depends on those pressure drops. This model captures the damper behavior in the preyield zone, in terms of the hysteresis. The authors do not evaluate the effects of the frequency in the model and the transient behavior of the force during changes in intensity of the electric field, which is important for control purposes. [9] presents a parametric dynamic model in which the pressure drops in the annular duct are calculated with respect to time. This model represents the hysteretic behavior of the ER damper in postyield zone and its increment due to the frequency, but the assessment of the model is done with constant conditions of frequency displacement and electric field. Another model is based on a lumped parameter method, in which the sections of the ER damper (upper chamber, lower chamber, annular duct, and connecting pipe) are divided into lumps and modeled with differential equations. This model predicts the nonlinear behavior of the ER damper in the preyield and postyield zones but depends on physical properties of the damper and it is sensitive to the initial conditions, [10].

Regarding the nonparametric models, [11] presents a polynomial equation with only three constants that can be fitted by least square estimation (LSE) methods; the force of the damper only depends on the velocity of the piston. The advantage of this model is the few number of constants but it does not seem to be very accurate; also it needs a set of constants for every field manipulation interval. Another approach is the Eyring model [12] which uses an Arcsinh function with shape parameters that depends on the electric field intensity and the frequency. This model can represent the behavior in both the preyield and the postyield zone but needs the identification of every parameter in each combination of frequency and field intensity; the accuracy of the model depends on how small are the considered intervals of the variables, but when changing the between this levels the model does not consider a transient response of the force. [13] introduces a neurofuzzy training algorithm to model the force of the ER damper, using the values of the acceleration and velocity of the damper; this model captures the nonlinear behavior of the ER damper with high level of accuracy, but the evaluation was done under very limited conditions.

Most of the models are dependent on internal physical properties of the damper, ER fluid, and its design; this makes the implementation of these models very restricted (i.e., confidential information). Our proposal considers general model that is customized based only on experimental data of the ER damper. The experimental system and Design of Experiments are shown in the next section.

3. Design of Experiments

A commercial ER damper was used, Figure 1(a). The damper has a stroke of ±150 mm and a force range of [−2500, 4500] N. The damper is actuated by a 2 module which is controlled by a 25 kHz pulse-width modulated (PWM) signal. The PWM duty cycle range was 10–80%. Since the ER damper needs to be operated with a voltage signal of 0–5 kV the 2 module proportionally transforms the duty cycle of PWM signal to voltage. Figure 1(b) shows the characteristic force-velocity (FV) diagrams at different PWM duty cycles.

The experimental setup, Figure 2(a), consists of three modules: (1) the acquisition system, which registers the displacement, velocity, damper force, and PWM signals using a National Instruments (NI) cDAC; (2) the hydraulic actuation system which consists of a piston that is actuated by a MTS 407 controller; and (3) the control system, which is used as an interface (control panel programmed in NI LabView) to operate the system.

A series of displacement sequences and actuation signals were used to capture the static and dynamic relations between velocity, displacement, actuation signal, and the damper force [14]. These sequences ensure the ER damper will be tested in the automotive domain. The sequences used for the displacement of the piston are road profile (RP), Figure 2(b), [15], and decreasing-amplitude stepped frequency sinusoidal (DSFS) signal, Figure 2(c), [16].

The RP sequence is used to test the ER damper under standard automotive conditions and represents the motion in a vehicle suspension when the car is driven through a specific surface. The RP smooth highway is the most common road for commercial vehicles. On the other hand, the DSFS signal is used to analyze the transient response and the hysteresis loops when changes in magnitude and frequency are

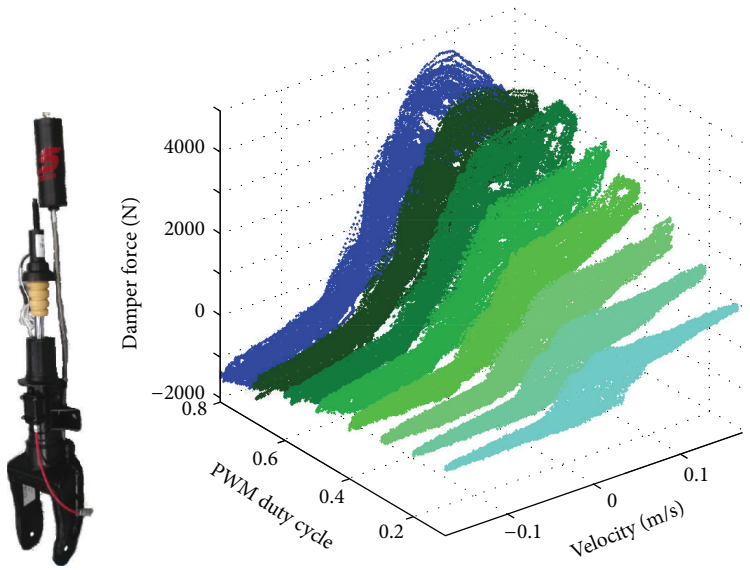

(a) SOBEN ER damper

(b) Characteristic FV diagrams

FIGURE 1: ER damper and its force-velocity diagrams.

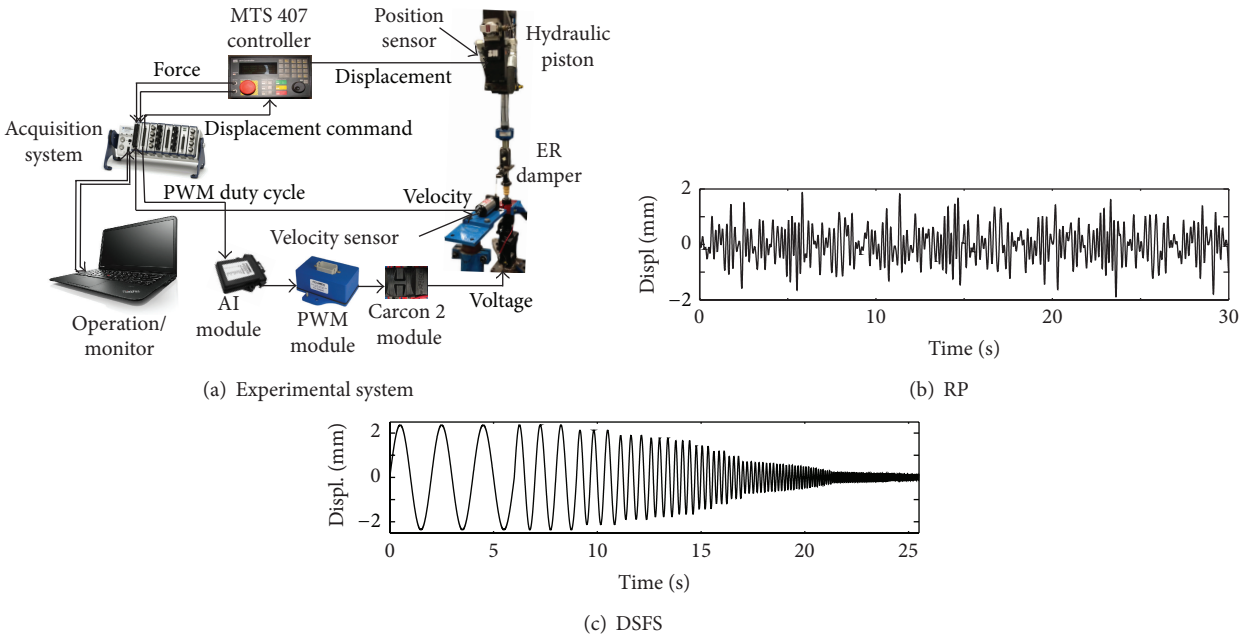

(a) Experimental system

(b) RP

(c) DSFS

FIGURE 2: Experimental system and displacement sequences (RP and DSFS).

present. The bandwidth of the DSFS displacement sequence is [0.5, 14.5] Hz wherein lie comfort and road holding specifications. In addition, DSFS sequence has a similar frequency spectrum experienced by automotive suspension systems.

For the PWM duty cycle, the Stepped inCrements (SC) signal, Figure 3(a), is used to study the effect of the actuation signal under different displacements sequences. Increased clock period signal (ICPS), Figure 3(b), and pseudorandom binary signal (PRBS), Figure 3(c), sequences are used to analyze the damper transient response under actuation signal variations. The ICPS is a signal with random amplitude variations, whereas the PRBS is a signal whose amplitude switches between two constant values with a random frequency.

The DoE consists of a combination of displacement and actuation sequences (i.e., 5 experiments). Experiment 1 (E_1) for characterization purposes uses the DSFS sequence repeated at each of the steps of the SC signal so that the damper could be excited in a wide range of displacements

Table 1: Design of experiments.

Experiment	Sequence	Displacement Amp. [mm]	Frequency [Hz]	Actuation signal	Purpose
E_1	DSFS	±1–±8	[0.5–14.5]	SC	Characterization
E_2	RP	±8	[0–3]	PRBS	Identification
E_3	RP	±8	[0–3]	ICPS	Identification
E_4	DSFS	±1–±8	[0.5–14.5]	ICPS	Identification
E_5	DSFS	±1–±8	[0.5–14.5]	PRBS	Identification

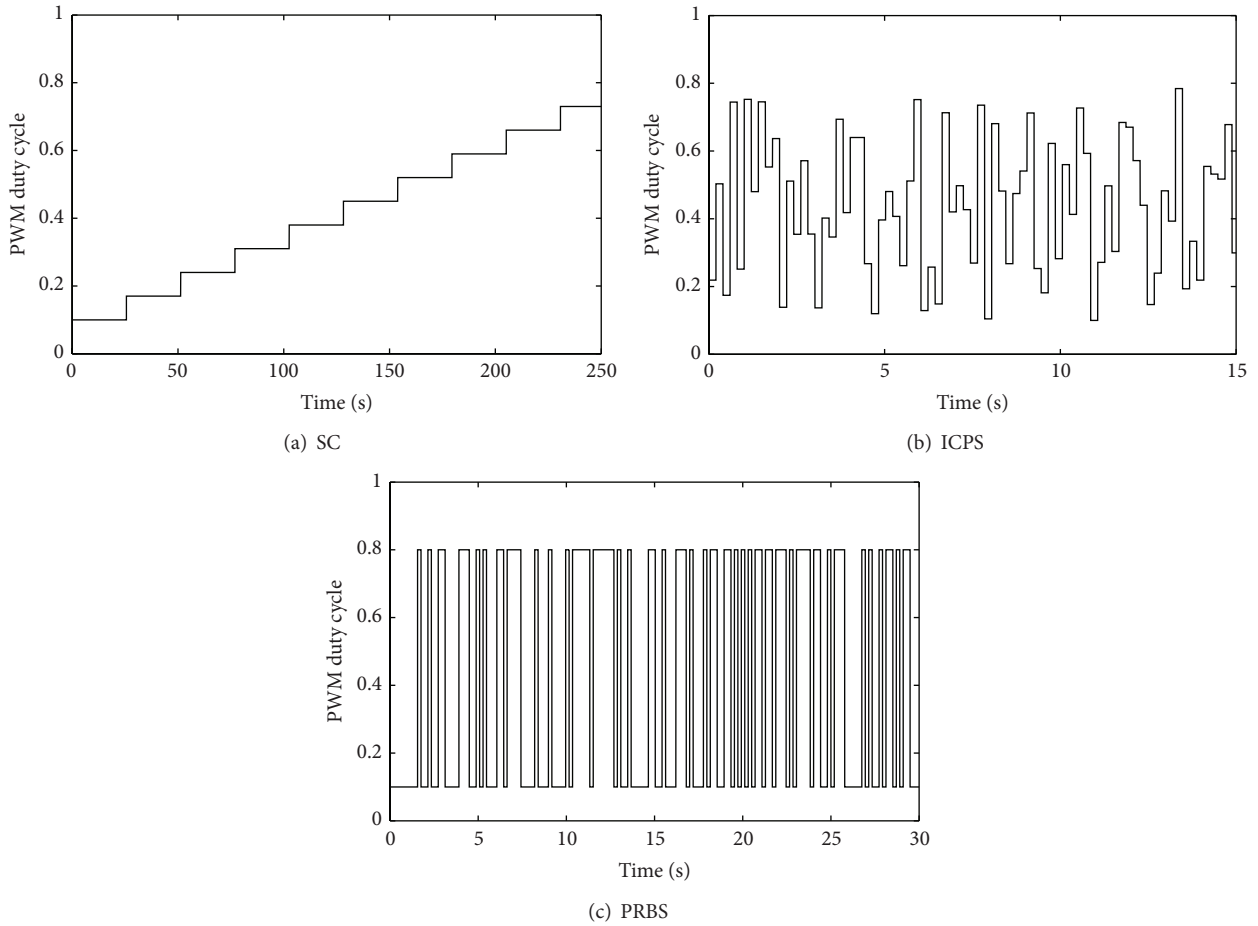

(a) SC

(b) ICPS

(c) PRBS

Figure 3: Actuation signals.

and forces. Experiments 2–5 ($E_2, \ldots, E_5$) for identification purposes are a combination of RP-DSFS sequences and PRBS-ICPS signals; while the DSFS explores a wide range of movement the RP only explores a limited one. For the actuation signal the use of a PRBS signal shows how the damper behaves when operated at its limit conditions; for the case of ICPS the full range of force was shown. Three replicas were implemented at a sampling frequency of 512 Hz, Table 1.

4. Proposed Method

The proposed method does not need a priori knowledge (i.e., physical properties, dimensional information, etc.) of the damper, Figure 4. In the DoE step, the experiments are defined on the automotive range of operation. In the characterization step, the dynamical characteristics of the damper behavior are analyzed based on the characteristic force-displacement (FD) and force-velocity (FV) diagrams. Then the general model is customized. In the identification step the model fits the 60% of the experimental data. In the validation step, the model is tested with the remaining 40% of the experimental data using the error-to-signal ratio (ESR) performance index.

4.1. Characterization. The ER damper force can be represented by two components: a passive component, which is present for all voltage input values, and a SA component,

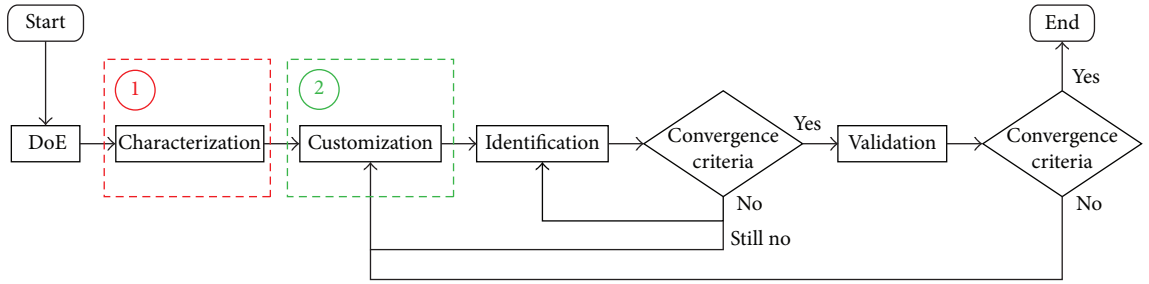

Figure 4: Proposed modeling method.

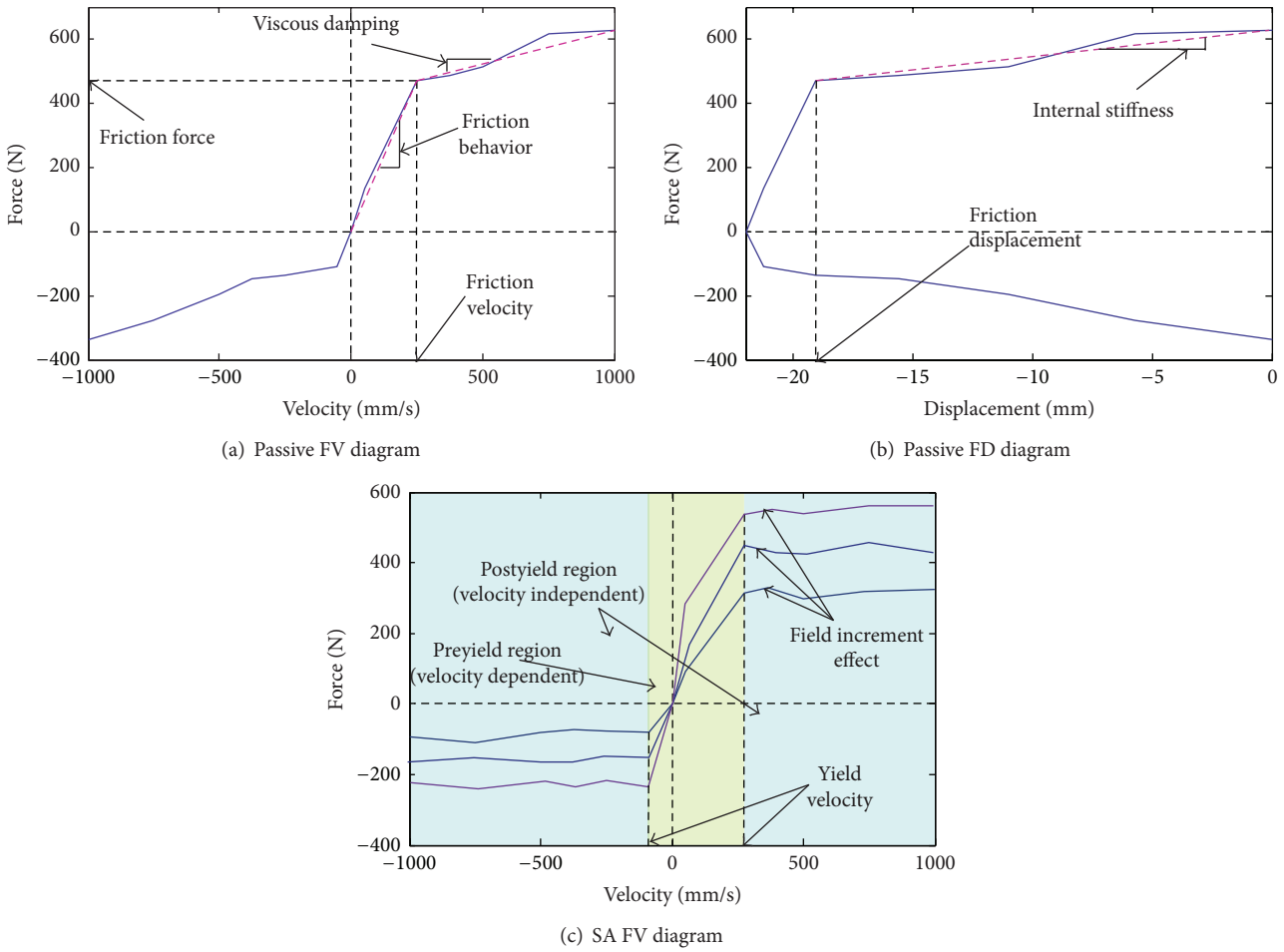

(a) Passive FV diagram

(b) Passive FD diagram

(c) SA FV diagram

Figure 5: Characteristics diagrams of a semiactive damper.

which depends on the actuation input [5]. The SA force component depends on the actuation signal as

$$F_{SA}(V) = F_D(V) - F_P, \quad (1)$$

where F_{SA} is the added force due to the manipulation signal V to de damper force F_D if a voltage V is applied and F_P is the measured damper force in an experiment with zero or minimum manipulation. The FV and FD diagrams are analyzed to find the characteristics that define the damper, Figure 5. The passive FV and FD experimental diagrams, Figures 5(a) and 5(b), are analyzed and the following characteristics can be identified:

(i) hysteresis: the observed hysteresis is considered significant, based on the dispersion of the force measurements (wider plot forms);

(ii) static friction: the passive force presents a drastic change of force at low velocities

(iii) viscous damping: it is the constant force gain that depends of the velocity

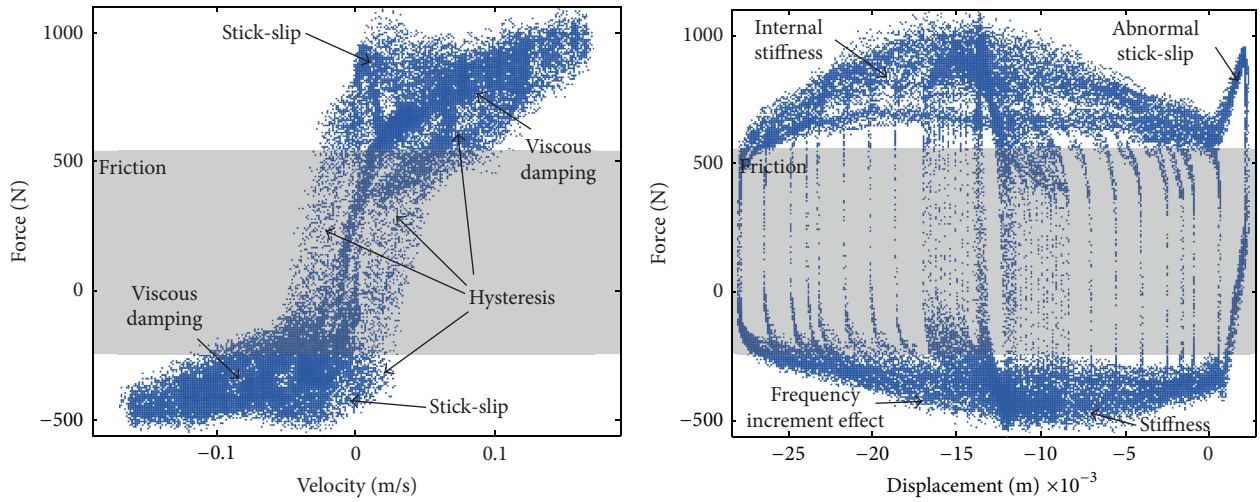

(a) Passive FD diagram

(b) Passive FV diagram

Figure 6: Characteristic diagrams of the ER damper passive behavior.

Table 2: Model terms used to represent the ER damper characteristics.

Characteristic	Observed diagram	Model term
Viscous damping	Passive FV	$c_p\dot{z}$
Stiffness	Passive FD	$k_p z$
Friction	Passive FV	f_{fr}
Hysteresis loop	Passive FV	$f_{h,z}$
Frequency dependent hysteresis	Passive FV	$f_{h,\dot{z}}, m_D$
Preyield zone	SA FV	$f_{\text{pre-}y,\dot{z}}$
Gain in force due to manipulation	SA FV	c_{SA}

(iv) stiffness: this characteristic is related to how much the gas in the accumulator can be compressed after defriction force has yielded.

Afterwards the SA diagram, Figure 5(c), is analyzed using (1). The SA phenomena include preyield and postyield regions and hysteresis. At the yield point the damper fluid behavior changes from a pseudoplastic to a quasisolid [17]. In the FV diagram the yield point is a Cartesian point where the damping force becomes independent of the velocity. The yield point defines where the SA damper operates: in preyield zone or in postyield zone. Also, at the postyield zone, an average force gain (FM) is obtained, based on the average value in which the yield of the force occurs at each manipulation value.

The characterization procedure was applied to the damper, using experiment E_1, Table 2. E_1 was selected because the DSFS displacement excitation signal explores all the realistic operational range of an automotive damper, in terms of frequency and displacement, and the SC actuation signal causes the damper to show its entire force range. E_1 allows observing the same dynamical effects of the ER damper caused by the excitation signal at different levels of actuation. Since this damper cannot be operated with no applied field, the sequence at 10% of duty cycle PWM will be considered passive.

Passive Behavior. Figure 6 shows the significant effects that are present in this ER damper operating in passive mode. From the FV diagram, Figure 6(a), it can be seen that this ER damper is asymmetrical; the maximum force in extension (positive velocity) is greater than the force generated in compression (negative velocity). The force has a velocity dependent component, which is also different in extension and compression. This damper presents significant hysteresis in all its operational range, being more notorious at low speed and in positive velocity. At low speed a friction component (~700 N) can be observed. This ER damper is subjected to the stick-slip phenomenon, especially in positive velocity; according to [5] this phenomenon appears in the ER damper as a force overshot when the flow changes its direction in the annular duct. In the FD diagram, Figure 6(b), an abnormal stick-slip appears as a peak, as well as effect of the frequency in the damper stiffness.

Semiactive Behavior. The behavior of the SA component of the force is presented in Figure 7. The relation between the SA force and the PWM duty cycle becomes evident; this relationship is asymmetrical, Figures 7(a) and 7(b). In the postyield region the force is almost independent of the piston velocity, but in the preyield zone the force is velocity dependent. Also at low speed the hysteresis loop in SA force is not significant, but as the velocity and the PWM duty cycle rise, the hysteresis rises too, Figure 7(a). In Figure 7(b) the stiffness of the damper is affected when the frequency is incremented; also it is notorious how the stick-slip phenomenon became greater as the manipulation increases. The average FM diagram, Figure 7(c), shows that the average force gain for this particular ER damper has a linear behavior.

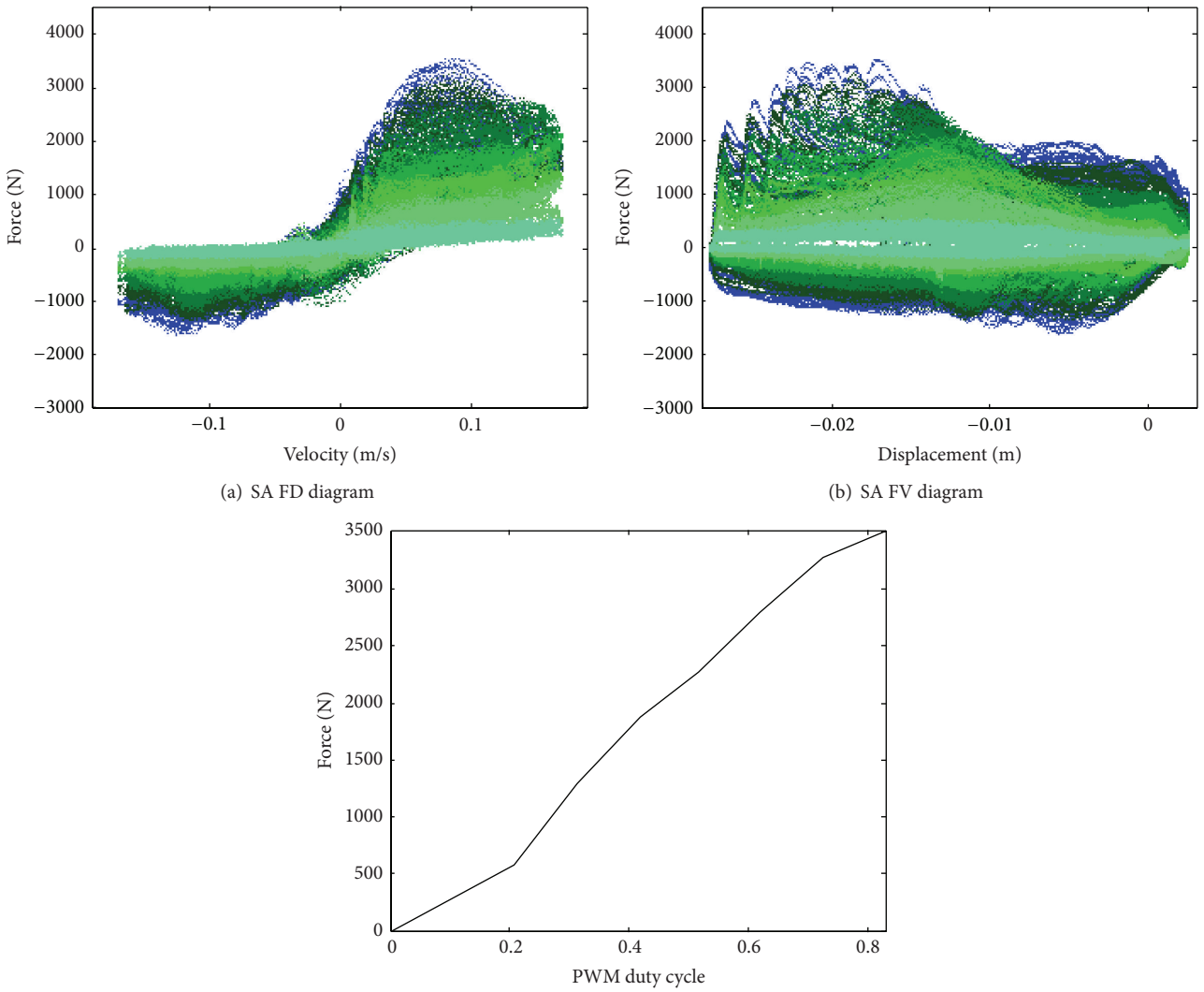

(a) SA FD diagram

(b) SA FV diagram

(c) SA average FM diagram

Figure 7: Characteristic diagrams of the ER damper SA behavior.

4.2. Customization. Equations (2), (3), and (4) are a general SA model which includes almost all the phenomena observed in SA dampers. Consider

$$F_D(V) = F_P + F_{\mathrm{SA}}(V), \tag{2}$$

where

$$F_P = f_0 + c_p\dot{z} + k_p z + m_D\ddot{z} + f_{\mathrm{fr}} + f_{h,z} + f_{h,\ddot{z}}, \tag{3}$$

$$F_{\mathrm{SA}}(V) = Vc_{\mathrm{SA}}\left[f_{\text{pre-}y,\dot{z},V} + f_{\text{pre-}y,z}\right] \tag{4}$$

with

$$f_{\mathrm{fr}} = f_f\left(\frac{v_f\dot{z} + x_f z}{1 + \left|v_f\dot{z} + x_f z\right|}\right),$$

$$f_{h,z} = f_{h,z}\left(\frac{v_{h,z}\dot{z} + x_{h,z}\,\mathrm{sign}(z)}{1 + \left|v_{h,z}\dot{z} + x_{h,z}\,\mathrm{sign}(z)\right|}\right),$$

$$f_{h,\ddot{z}} = f_{h,\ddot{z}}\left(\frac{v_{h,\ddot{z}}\dot{z} + x_{h,\ddot{z}}\,\mathrm{sign}(\ddot{z})}{1 + \left|v_{h,\ddot{z}}\dot{z} + x_{h,\ddot{z}}\,\mathrm{sign}(\ddot{z})\right|}\right),$$

$$f_{\text{pre-}y,\dot{z},V} = \left(\frac{v_{\text{pre-}y,\dot{z},I}\dot{z}V}{1 + \left|v_{\text{pre-}y,\dot{z},I}\dot{z}V\right|}\right),$$

$$f_{\text{pre-}y,z} = \left(\frac{x_{\text{pre-}y,z}z}{1 + \left|x_{\text{pre-}y,z}z\right|}\right). \tag{5}$$

Equation (3) describes the passive force (F_P). The passive force component f_0 is an initial compensation force generated by the accumulator, c_p is the viscous damping coefficient which describes the linear viscous damping of the Newtonian fluids, k_p is the stiffness coefficient which is the characteristic of linear elastomers, m_D is the virtual damper mass, f_{fr} is the damping force due to friction, and $f_{h,z}$, $f_{h,\dot{z}}$ model the hysteresis [18–20]. Equation (4) represents the SA force F_{SA},

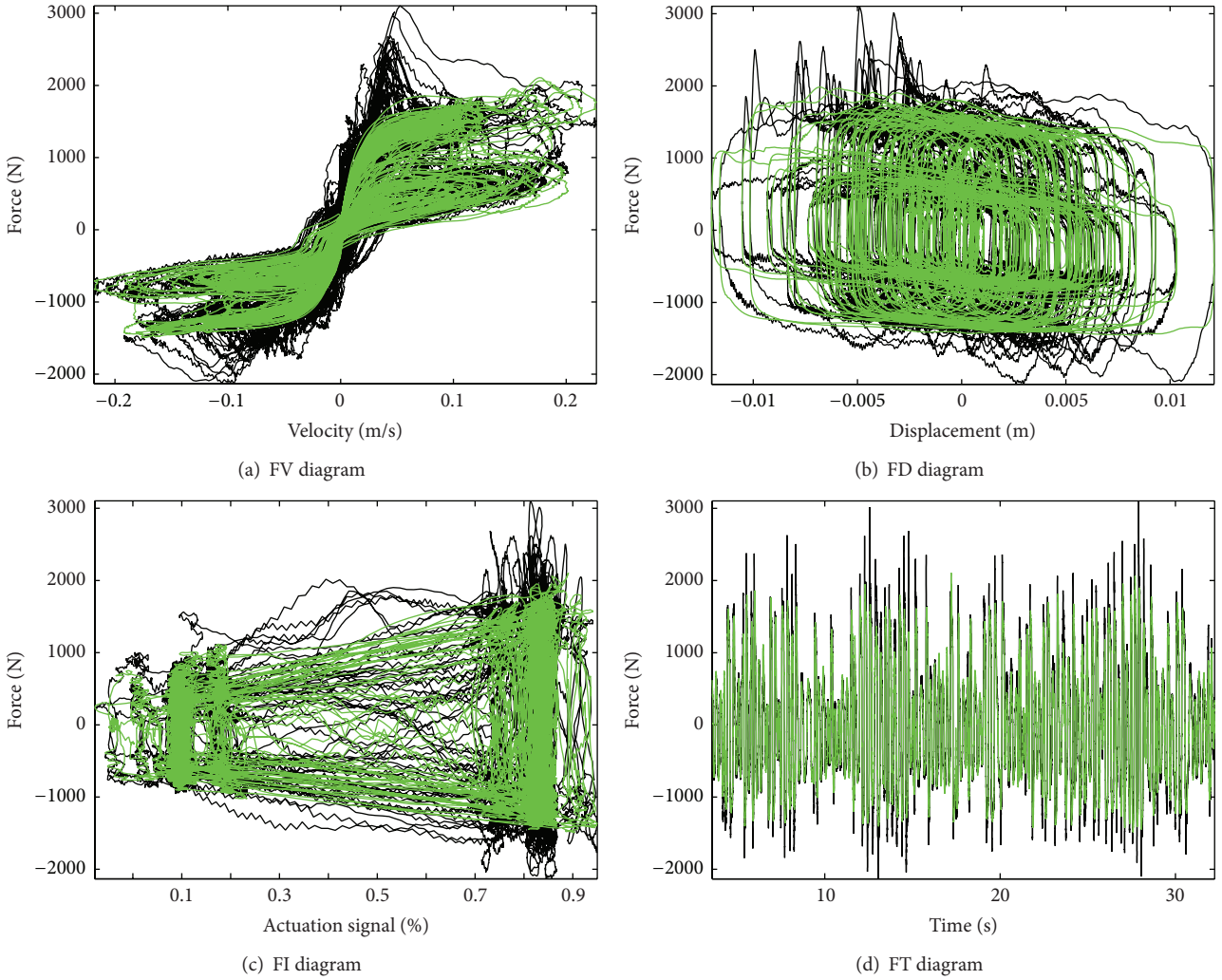

(a) FV diagram (b) FD diagram

(c) FI diagram (d) FT diagram

Figure 8: Comparison of estimated (green) and experimental (black) data of based on E_2.

where V is the manipulation applied to the damper, c_{SA} is the force gain due to manipulation, and $f_{\text{pre-}y,z}$, $f_{\text{pre-}y,\dot{z},I}$ describe the behavior of the damper in the preyield zone. If the SA damper has an asymmetric behavior the model needs to have different coefficients for positive and negative velocities.

In these equations, the use of the tanh function is replaced with the so-called squash function: $x/(1+|x|)$. This function has the advantage of been lighter for computing while reproducing almost the same pattern as the tanh.

Depending on the physical characteristics of the ER damper, (3), (4) are customized so that only the required terms are considered to preserve an accurate representation while simplifying the model structure, Table 2. For the passive force, Figure 6, friction, stiffness, and viscous damping were observed. Frequency dependent hysteresis was also present in the ER damper response. The SA damper force, Figure 7, presents a sigmoid behavior without significant hysteresis. The preyield and postyield zones depend on the actuation signal but only the preyield zone depends on the damper velocity.

Based on those observations, (3), (4) were customized for this ER damper; the following asymmetric model for the ER damper is proposed:

$$F_P = f_0 + c_p\dot{z} + k_p z + m_D\ddot{z} + f_{\text{fr}}, \tag{6}$$

$$F_{\text{SA}} = Vc_{\text{SA}}\left[f_{\text{pre-}y,\dot{z},V} + f_{\text{pre-}y,z}\right]. \tag{7}$$

5. Modelling

Based on the previous analysis, the identification and validation steps are relatively standard.

5.1. Identification. The model parameters were fitted using the LSE method. Since the ER damper behavior is asymmetric, the model parameters have different values for positive and negative velocities. Three replicas of each experiment were used to evaluate the performance of the customized model. Figures 8 and 9 show the experimental and estimated FV, FD, FE, and FT diagrams generated from experiments E_2 and E_3, respectively.

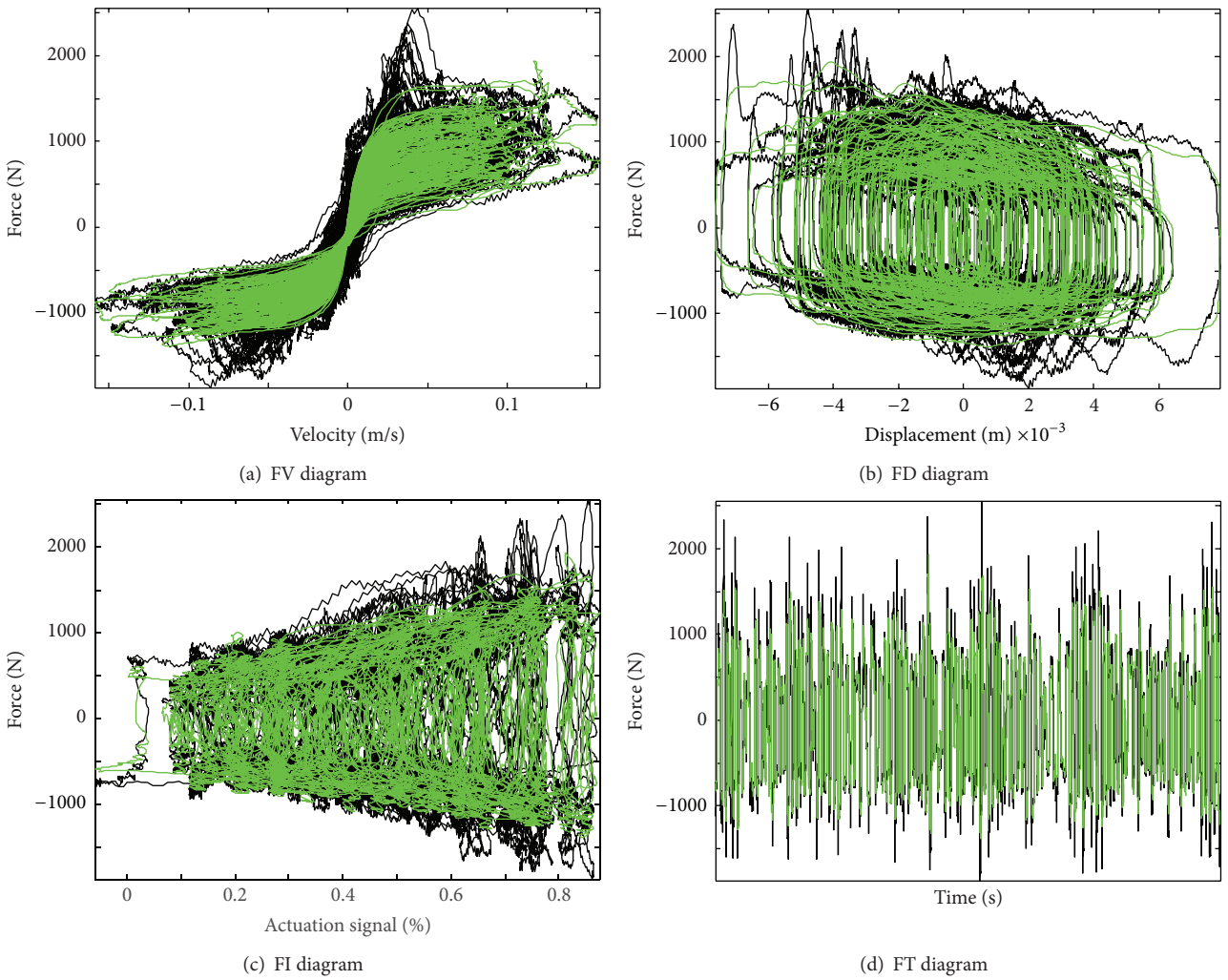

(a) FV diagram (b) FD diagram

(c) FI diagram (d) FT diagram

Figure 9: Comparison of estimated (green) and experimental (black) data based on E_3.

Based on Figures 8 and 9 the customized model correctly describes the nonlinear behavior of the ER damper and the effect of the actuation signal, and estimated data looks similar to the real data. However, this model was unable to describe the stick-slip phenomenon, Figures 8(a) and 9(a), in the FV diagrams; they are the force peaks around 0.04 and −0.05 m/s that the model cannot mimic. In Figures 8(b) and 9(b) it can be seen that the model can represent the rigidity of the damper, but in the same way as in Figures 9(a) and 10(a) the stick-slip phenomenon appears again. This force peaks appear also in Figures 8(c) and 8(d) and Figures 9(c) and 9(d), where the real data differ from the estimated data in the top and bottom zones of the diagrams.

For quantitative validation purposes the error-to-signal ratio (ESR) performance index was selected. It represents the ratio between the variance of the estimation error and the variance of the experimental damper force [21]. If the value of the ESR is 0, it indicates that the model estimates exactly the damper force; however, a value of 1 indicates that the model only predicts the mean value of the damper force.

The performance indexes for all the experiments (customized and full models) are shown in Table 3. It can be observed that the values of the ESR are consistent in the three replicas, with an average difference of 3%; therefore, for the following analysis only the first replica will be considered. It can be observed that in almost all experiments the customized model shows same results as the full model, with the exception of E_5. This is because E_5 uses the DSFS

Table 3: ESR index for the full and customized models.

Experiment	Replica 1	Replica 2	Replica 3
Customized model			
E_2	0.0741	0.0749	0.0716
E_3	0.062	0.0627	0.0654
E_4	0.1284	0.1337	0.1315
E_5	0.1558	0.1494	0.1416
Full model			
E_2	0.0730	0.0739	0.0719
E_3	0.0674	0.0661	0.0681
E_4	0.1258	0.1353	0.1330
E_5	0.0797	0.0762	0.0744

Table 4: Performance indices for different datasets.

Experiment used for validation	Force variance $\sigma^2 \times 10^5$	Experiment used for identification			
		E_2	E_3	E_4	E_5
E_2	8.39	0.0741	0.0811	0.1988	0.1065
E_3	6.50	0.0676	0.0620	0.1762	0.1154
E_4	5.79	0.3041	0.0614	0.1258	0.1664
E_5	6.13	0.2546	0.3032	0.1727	0.1558
Average		**0.1751**	**0.1269**	**0.1684**	**0.1360**

displacement sequence with the PRBS control signal. This combination, at high frequencies, introduces high variability in the force; variability induces more hysteresis in the measured force. Since the terms related with the hysteresis have been taken out from the model, when the hysteresis is predominant, the customized model is not able to reproduce the force as correct as the full model.

5.2. Validation. The first step of the validation process is to prove that the terms discarded have little influence in the modeling performance; this is done by comparing the performance indexes obtained with the full model, (3), (4), versus the ones obtained with the customized model, (6), (7).

Table 3 shows that the performance indices of the customized model are very similar to the full model; for both models the ESR indices are low. Therefore, the discarded terms in the customized model has little effect in the response of this damper; this is consistent with the results obtained in the characterization step. Experiments E_2 and E_5 have a greater ESR index when compared with the ones achieved in experiments E_3 and E_4, respectively. This is because the small changes in the ICPS manipulation signal have little effect on the variability of the force; on the other hand the PRBS manipulation signals, which are steps of 10% to 80% and vice versa, cause the force to experiment greater variability that increments the effects of some phenomena as stick-slip and hysteresis. Since in the model customization step those terms were excluded, the model was less effective in capturing those highly hysteric behaviors. This explains why in the experiment E_5 the ESR is almost the double of the one achieved with the full model.

A second validation procedure was to prove the extrapolation ability. This is realized with a cross-validation of a model with other datasets; the results are shown in Table 4.

It was observed that the customized model can be extrapolated to other signals different from those used in the identification stage. The best average performance was obtained by the experiment E_5 (even though the ESR for each experiment is not the smallest). This is result of the actuation and manipulation signals used in that experiment, because the DSFS signal captures best the dynamical behavior of the damper in its whole range of operation while the RP only explores a limited zone. The ICPS covers the whole force range of the shock absorber while the PRBS only captures the limits of the force range.

The two validation procedures show that the customized model performance is as the full model. Also, the customized model can extrapolate the results for different experimental data.

6. Results

These results were also validated with two-dimensional density plots. The density plots are scatter plots that use different colors to indicate the density of incidences in different zones of the diagram; blue color indicates a lower number of occurrences (i.e. data samples), whereas red indicates a higher number. The FD, FV, and FM density plots with the customized model and experimental data are compared, Figure 10.

According to [22], since the experiment is a RP the zones with higher density of occurrences should be at low velocities for the FV diagram; in the case of the FD diagrams these zones should be in the small displacement range; on the other hand this experiment has a PRBS actuation signal; therefore the higher density zones must be in the ends of the control signal (0.1 and 0.8). The FV diagram of the estimated data, Figure 10(b), is similar to the one obtained with experimental data, Figure 10(a), but because the stick-slip phenomenon is not considered by the model, the estimated force does not present the peaks around 0.04 and −0.05 m/s observed in experimental data. For the FD diagrams, the friction zone is well defined in the model, Figure 10(d); this means, that in the zone of the y-axis between ±0.2, there should be little incidences. Also, the two levels of force, caused by the PRBS signal, should be clearly defined as well. In the case of the FM diagrams, Figures 10(e) and 10(f), only four points should be well define, since only two levels of current were used.

In order to analyze the effectiveness of the customized model, a comparative analysis with other two well-known models was carried out: the Choi parametric model [23] and the Eyring-plastic model [12]. The Choi parametric model is based on the physical characteristics of the ER damper. It is defined as follows:

$$F_D = k_e z + c_e \dot{z} + F_{\mathrm{ER}} \operatorname{sign}(\dot{z}) \tag{8}$$

with

$$F_{\mathrm{ER}} = \left(A_p - A_r\right) P_{\mathrm{ER}}, \quad P_{\mathrm{ER}} = d\alpha E^{\beta}, \qquad k_e = \frac{A_r^2}{C_g}, \qquad c_e = \left(A_p - A_r\right)^2 \mathrm{Re}, \tag{9}$$

where A_p and A_r are the piston and rod areas, respectively, C_g is the gas compliance, R_c is the flow resistance due to

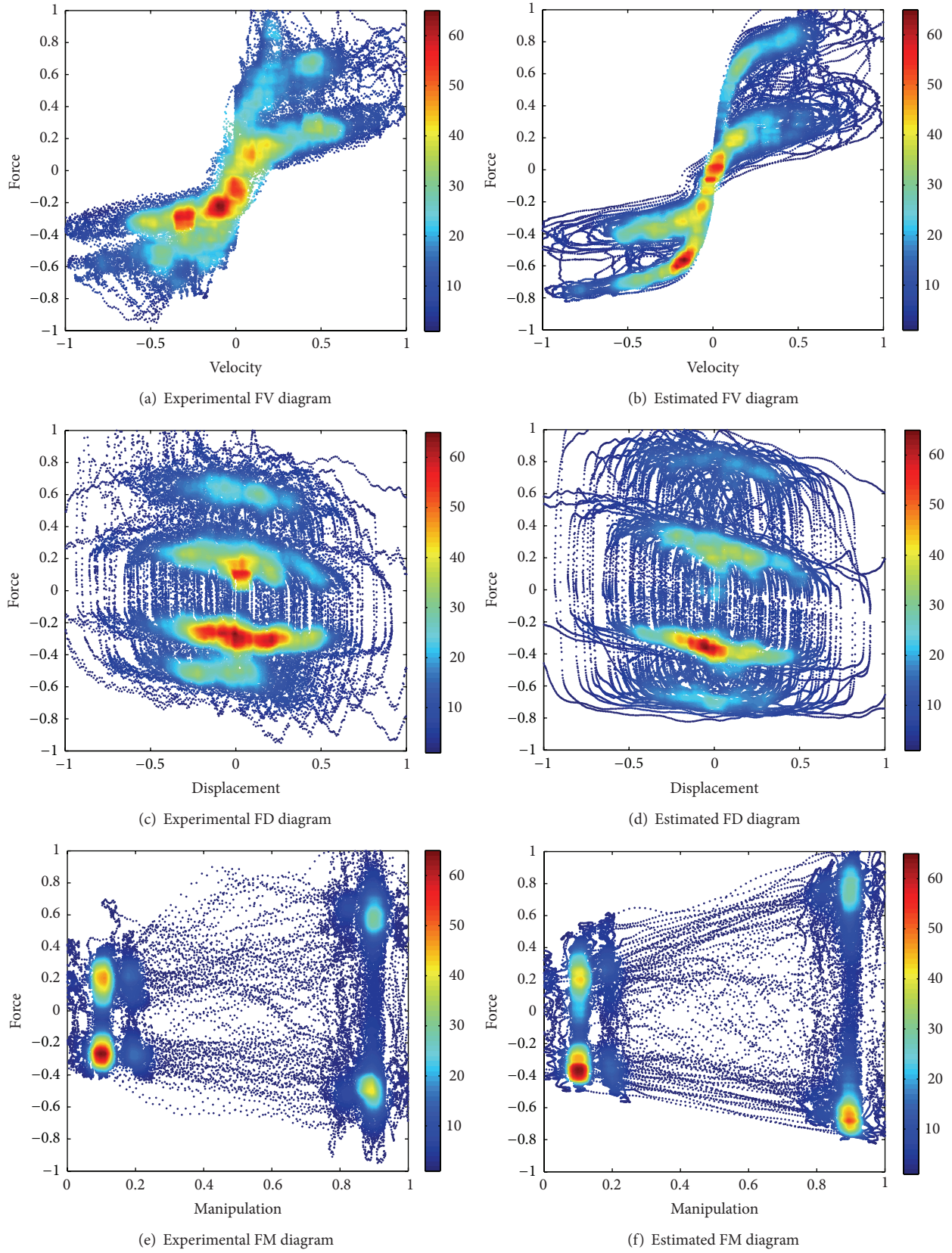

(a) Experimental FV diagram

(b) Estimated FV diagram

(c) Experimental FD diagram

(d) Estimated FD diagram

(e) Experimental FM diagram

(f) Estimated FM diagram

Figure 10: Density plots for experimental and estimated data.

Table 5: Comparison of ER damper models.

Model	Choi parametric model	Eyring-plastic model	Customized model
Parameters	4	7	20
Inputs	$z, \dot{z}$	$z, \dot{z}$	$z, \dot{z}, \ddot{z}$
Actuation signal as input	Yes	No	Yes
Hysteresis	No	Yes	Yes

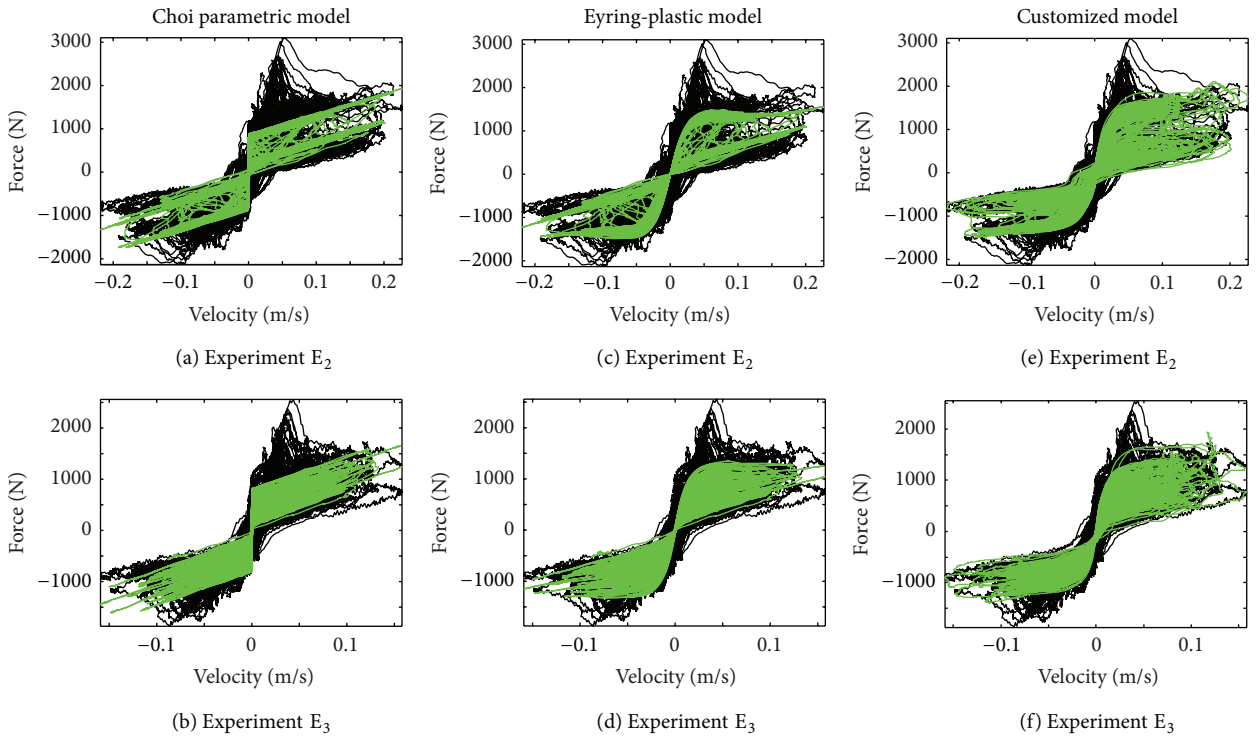

Figure 11: Comparison of models performance based on FV diagrams.

the velocity of the ER fluid, P_{ER} is the pressure drop due to the field-dependent yield stress, E is the applied electric field, d is a constant related to the geometry of the electrode, and α and β are experimentally determined constants which characterize the yield stress of the ER fluid.

In the Eyring-plastic model the force is considered a nonlinear function of the velocity:

$$F_D = F_\alpha \left[\operatorname{arcsinh}\left(\lambda_1 \dot{z} - \lambda_2 z\right)\right]\left(1 + \beta_1 e^{-\beta_2 |\dot{z}|}\right) + c - 1\dot{z} + c_3 \dot{z}^3, \tag{10}$$

where λ_1 defines the slope of the response in the preyield region, λ_2 defines the preyield hysteresis loop, F_α is related to the yield force amplitude, β_1, β_2 are yield force correction factors, and c_1, c_3 model the damping in the postyield region. The seven parameters are functions of the excitation frequency and electric field. Table 5 summarizes the different features of the models.

All the analyzed models are nonlinear and depend on the damper displacement (z) and velocity ($\dot{z}$). Only the customized model includes the acceleration $\ddot{z}$ as input. The Choi parametric model and the customized model explicitly include the actuation signal in the model structure whereas in the Eyring-plastic model the parameters are undefined functions of the actuation signal.

Table 6: Performance indices of the ER damper models.

Model	Experiment		
	E_2	E_3	E_4
Choi parametric model	0.1337	0.1164	0.2222
Eyring-plastic model	0.0996	0.0816	0.1996
Customized model	**0.0714**	**0.0642**	**0.1284**

These models were identified using the same data and algorithms, Table 6. Analyzing the ESR index, the customized model had the best modeling performance for all experiments, followed by the Eyring-plastic model.

Figure 11 compares the FV diagrams for each model in experiments E_2 and E_3. The Choi parametric model, Figures 11(a) and 11(b), does not estimate correctly the hysteresis and nonlinearities of the damping force, but the levels of force caused by the changes in the manipulation signal are notorious. The Eyring-plastic model, Figures 11(c) and 11(d),

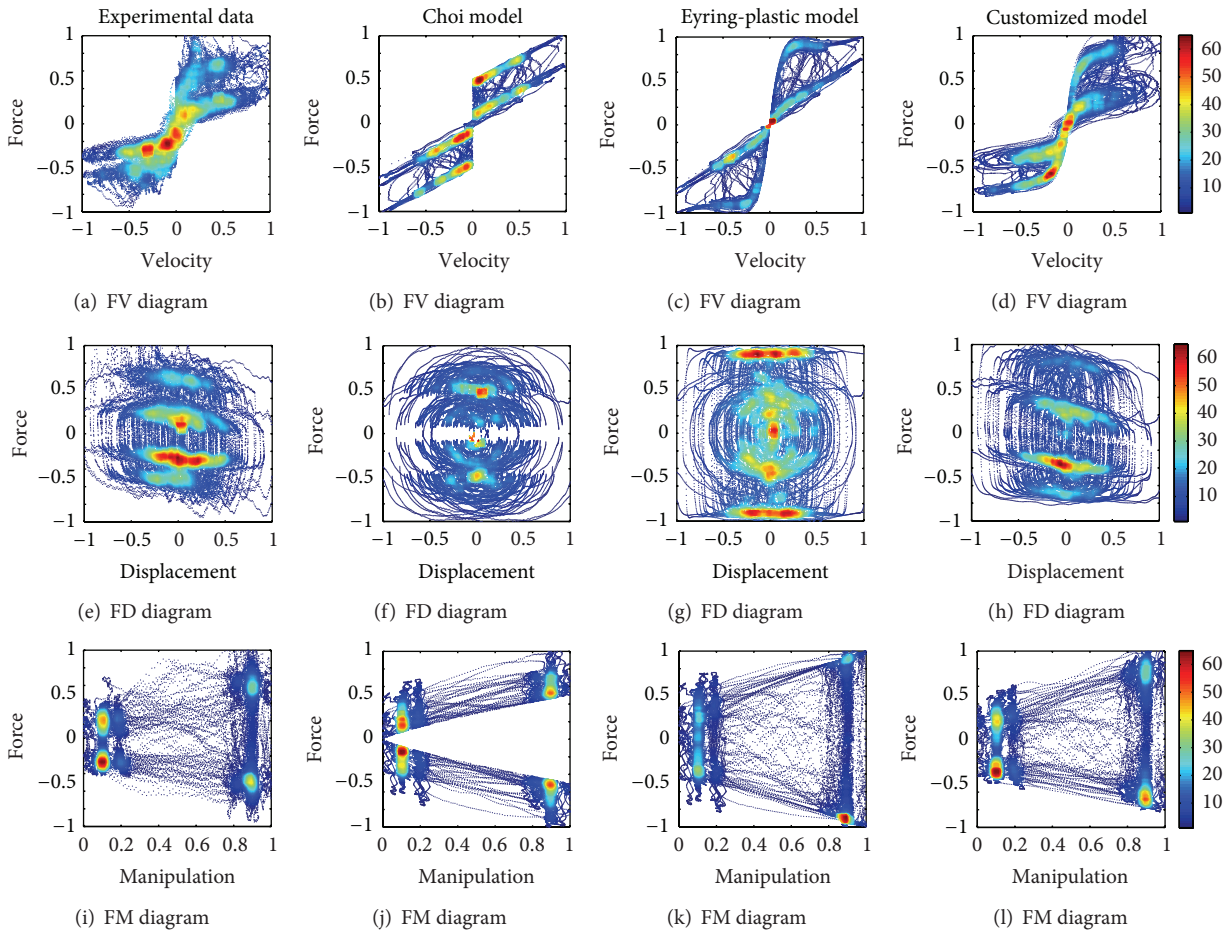

FIGURE 12: Density plots of experimental and estimated data for different models (experiment E_2).

has acceptable results at high velocities, but at low velocities (±0.02 m/s) it does not capture the hysteresis effect correctly. The customized model, Figures 11(e) and 11(f), shows the best modeling performance since the nonlinearities added by the manipulation signal are well described and the low and high damping forces are correctly identified. None of the analyzed models consider the stick-slip effect so the force peaks around 0.04 and −0.05 m/s are not reproduced by any of them.

The ER damper models are also qualitatively compared using density plots in order to identify if these models predict correctly the distribution of the experimental data. Figure 12 presents a comparison of the density plots of experiment E_2. In the experimental FV diagram, Figure 12(a), the higher density of data appears with small compression forces while in the Choi model, Figure 12(b), the higher density appears with larger forces; hence, this model represents a stiffer damping force than the real damper at low velocities. In the Eyring-plastic model FV diagram, Figure 12(c), the higher density appears with zero force; therefore the model generates smaller forces than the real damper with low velocities. Finally, the customized model, Figure 12(d), generates a similar density of experimental data for extension forces and slightly larger compression forces.

In the FD diagram the experimental data presents higher density with small forces, especially in compression, Figure 12(e). The Choi model presents higher density in extension forces with zero displacement; thus it generates larger forces with small displacements, Figure 12(f). This model also produces larger compression forces with large displacements. In contrast with the experimental data, in the Eyring-plastic model the higher density appears with large forces and exhibits a saturation, Figure 12(g); hence the Eyring-plastic model produces smaller forces with large displacements than the real damper. Finally, the customized model, Figure 12(h), produces slightly higher forces at low frequencies and a density distribution similar to the experimental data.

The FM diagram is important for control systems purposes. A model with the same shape and density distribution to the experimental data is required in order to compute a right manipulation to achieve a desired force. Since in experiment E_2 a PRBS actuation signal was used, the FM diagram mostly exhibits two manipulation values, Figure 12(i). All the models generate smaller forces with a manipulation of 90% where the stick-slip effect is more evident. Nonetheless, the FM diagram obtained with the customized model resembles the experimental data the most. The Choi and Eyring-plastic models present smaller forces than the customized model. The Choi model is not able to generate small forces due to the use of a discontinuous function; this explains why this model

Table 7: Execution times of the ER damper models.

Model	Time [s]
Choi parametric model	0.1500
Eyring-plastic model	0.1970
Customized model (squash)	0.3093
Customized model (tanh)	0.3600
Full model	0.3950

could not predict the small forces present on the experimental data.

Since the model should be well suited for real time implementations, there was another comparative test done to all the models. This test consists in measuring the time that the model takes to compute a vector of data points; in this case the selected vector contains 58,123 data points. The results of this test are presented in Table 7, and each point is the average of 3 replicas of the test. For comparison purposes there are included the full model and the customized model using the tanh function instead of the squash function.

The results show, as expected, that the Choimodel spends less than half the time (0.15 s) than the customized model (0.3093 s), but its ESR index is almost twice the index of the customized model. The Eyring-plasticmodel spends 33% less time (0.197 s) than the customized model, but its ESR index is more than 30% bigger. Even if the customized model lasts longer to be computed its precision is much better. Comparing the customized model using the tanh function its time is 20% less, and as expected the time to compute the full model is 30% more.

7. Conclusions

A method for modeling ER dampers was proposed. The proposal does not need prior knowledge of the damper such as physical properties, dimensions, and so forth, just experimental data. The main contribution of this method is the simplicity that by analyzing the experimental data (i.e., in the form of characteristic diagrams) the ER damper can be modelled with a general equation; then it can be customized to obtain a simple model that captures the real behavior of a damper.

Based on design of experiments (DoE), the representative behavior of the damper into the automotive domain can be obtained. The resultant model proves its accuracy with an error-to-signal ratio (ESR) of 15.5% in the worst case and an average of 12.7% when extrapolating other experiments. Also, when compared with well-known models, the results have better performance, an average of 44.5% less than the Choi parametric model and 28.4% less than the Eyring-plastic model. Additionally, the density plots allow a qualitative comparison of the results, giving same conclusions.

The customized model ends with a short equation with high performance. Compared with well-known approaches, the simplicity of the method that does not demand a specialized background of design and modeling of electrorheological dampers is the main important contribution.

Conflict of Interests

The authors declare that there is no conflict of interests regarding the publication of this paper.

Acknowledgments

Authors thank *Tecnológico de Monterrey* and *national science and technology council of México* through the bilateral Projects (no. 142183 México-Spain and PCP-03/10 México-France) because of their partial support.

References

[1] T. D. Gillespie, *Fundamentals of Vehicle Dynamics*, SAE, Warrendale, Pa, USA, 1992.

[2] B. F. Spencer Jr., S. Dyke, M. Sain, and J. Carlson, "Phenomenological model for magneto-rheological dampers," *Journal of Engineering Mechanics*, vol. 123, no. 3, pp. 230–238, 1997.

[3] T. Butz and O. von Stryk, "Modelling and simulation of electro and magneto-rheological fluid dampers," *Journal of Applied Mathematics and Mechanics*, vol. 82, no. 1, pp. 3–20, 2002.

[4] R. Stanway, J. L. Sproston, and A. K. El-Wahed, "Applications of electro-rheological fluids in vibration control: a survey," *Smart Materials and Structures*, vol. 5, no. 4, pp. 464–482, 1996.

[5] J. Dixon, *The Shock Absorber Handbook*, John Wiley & Sons, New York, NY, USA, 2007.

[6] S. B. Choi, Y. T. Choi, E. G. Chang, S. J. Han, and C. S. Kim, "Control characteristics of a continuously variable ER damper," *Mechatronics*, vol. 8, no. 2, pp. 143–161, 1998.

[7] S. B. Choi, H. K. Lee, and E. G. Chang, "Field test results of a semi-active ER suspension system associated with skyhook controller," *Mechatronics*, vol. 11, no. 3, pp. 345–353, 2001.

[8] S. R. Hong, S. B. Choi, Y. T. Choi, and N. M. Wereley, "A hydromechanical model for hysteretic damping force prediction of ER damper: experimental verification," *Journal of Sound and Vibration*, vol. 285, no. 4-5, pp. 1180–1188, 2005.

[9] Q.-H. Nguyen and S.-B. Choi, "Dynamic modeling of an electrorheological damper considering the unsteady behavior of electrorheological fluid flow," *Smart Materials and Structures*, vol. 18, no. 5, Article ID 055016, 2009.

[10] Q.-H. Nguyen and S.-B. Choi, "A new approach for dynamic modeling of an electrorheological damper using a lumped parameter method," *Smart Materials and Structures*, vol. 18, no. 11, Article ID 115020, 2009.

[11] S.-M. Chen and C.-G. Wei, "Experimental study of the rheological behavior of electrorheological fluids," *Smart Materials and Structures*, vol. 15, no. 2, pp. 371–377, 2006.

[12] L. Bitman, Y. T. Choi, S. B. Choi, and N. M. Wereley, "Electrorheological damper analysis using an Eyring-plastic model," *Smart Materials and Structures*, vol. 14, no. 1, pp. 237–246, 2005.

[13] S. D. Nguyen and S.-B. Choi, "A new neuro-fuzzy training algorithm for identifying dynamic characteristics of smart dampers," *Smart Materials and Structures*, vol. 21, no. 8, Article ID 085021, 2012.

[14] J. de-J. Lozoya-Santos, R. Morales-Menendez, R. Ramirez-Mendoza, J. C. Tudón-Martinez, O. Sename, and L. Dugard, "Magnetorheological damper—an experimental study," *Journal of Intelligent Material Systems and Structures*, vol. 23, no. 11, pp. 1213–1232, 2012.

[15] D. Kowalski, M. Rao, J. Blough, and S. Gruenberg, "The effects of different input excitation on the dynamic characterization of an automotive shock absorber," in *Proceedings of the SAE Noise and Vibration Conference and Exhibition*, Traverse City, Mich, USA, 2001, SAE paper no. 2001-01-1442.

[16] C. Boggs, L. Borg, J. Ostanek, and M. Ahmadian, "Efficient test procedures for characterizing MR dampers," in *Proceedings of the ASME International Mechanical Engineering Congress and Exposition (IMECE '06)*, pp. 173–178, Chicago, Ill, USA, November 2006.

[17] F. Irgens, *Continuum Mechanics*, Springer, Berlin, Germany, 2008.

[18] S. Guo, S. Yang, and C. Pan, "Dynamic modeling of magneto-rheological damper behaviors," *Journal of Intelligent Material Systems and Structures*, vol. 17, no. 1, pp. 3–14, 2006.

[19] N. M. Kwok, Q. P. Ha, T. H. Nguyen, J. Li, and B. Samali, "A novel hysteretic model for magnetorheological fluid dampers and parameter identification using particle swarm optimization," *Sensors and Actuators A: Physical*, vol. 132, no. 2, pp. 441–451, 2006.

[20] S. Cesmeci and T. Engin, "Modeling and testing of a field-controllable magnetor-rheological fluid damper," *International Journal of Mechanical Sciences*, vol. 52, no. 8, pp. 1036–1046, 2010.

[21] S. M. Savaresi, S. Bittanti, and M. Montiglio, "Identification of semi-physical and black-box non-linear models: the case of MR-dampers for vehicles control," *Automatica*, vol. 41, no. 1, pp. 113–127, 2005.

[22] N. Fukushima, K. Hidaka, and K. Iwata, "Optimum characteristics of automotive shock absorbers under various driving conditions and road surfaces," *JSAE Review*, pp. 62–69, 1983.

[23] S.-B. Choi, Y.-M. Han, and K.-G. Sung, "Vibration control of vehicle suspension system featuring ER shock absorber," *International Journal of Applied Electromagnetics and Mechanics*, vol. 27, no. 3, pp. 189–204, 2008.